frontiers | Frontiers in Climate

TYPE Original Research
PUBLISHED 31 October 2022
DOI 10.3389/fclim.2022.996343

OPEN ACCESS

EDITED BY
Chunzai Wang,
South China Sea Institute of Oceanology (CAS), China

REVIEWED BY
Ming Feng,
Commonwealth Scientific and Industrial Research Organisation (CSIRO), Australia
Takeshi Doi,
Japan Agency for Marine-Earth Science and Technology (JAMSTEC), Japan
Lei Zhang,
South China Sea Institute of Oceanology (CAS), China

*CORRESPONDENCE
Dongliang Yuan
dyuan@qdio.ac.cn

SPECIALTY SECTION
This article was submitted to Predictions and Projections, a section of the journal Frontiers in Climate

RECEIVED 17 July 2022
ACCEPTED 10 October 2022
PUBLISHED 31 October 2022

CITATION
Xu T, Yuan D and Wang J (2022) Assessment of the oceanic channel dynamics responsible for the IOD-ENSO precursory teleconnection in CMIP5 climate models. *Front. Clim.* 4:996343. doi: 10.3389/fclim.2022.996343

Assessment of the oceanic channel dynamics responsible for the IOD-ENSO precursory teleconnection in CMIP5 climate models

Tengfei Xu[1,2,3], Dongliang Yuan[4,1,2,3]* and Jing Wang[4]

[1]Key Laboratory of Marine Science and Numerical Modeling, First Institute of Oceanography, Ministry of Natural Resources, Qingdao, China, [2]Laboratory for Regional Oceanography and Numerical Modeling, Pilot National Laboratory for Marine Science and Technology, Qingdao, China, [3]Shandong Key Laboratory of Marine Science and Numerical Modeling, Qingdao, China, [4]Key Laboratory of Ocean Circulation and Waves, Institute of Oceanology, Chinese Academy of Science, Qingdao, China

Existed studies have suggested a precursory relation between Indian Ocean Dipole (IOD) and El Niño and the Southern Oscillations (ENSO) with 1-year time lag. The underlying mechanisms were attributed to atmospheric bridge and/or oceanic channel processes. In this study, the oceanic channel dynamics in 23 climate models of the Coupled Model Intercomparison Project phase 5 (CMIP5) are assessed by correlation analyses in comparison with observations. The results show that the lag correlations between the IOD and ENSO anomalies associated with oceanic channel are significant, suggesting important role of oceanic channel dynamics in the cross-basin teleconnection in the analyzed CMIP5 models, consistent with observational analyses. In comparison, the correlations associated with atmospheric bridge are highly dispersive among the models and generally inconsistent with the observational analyses, suggesting model deficiencies. In a single climate model, the lag correlations associated with oceanic channel dynamics are consistent among different ensemble experiments, whereas those associated with atmospheric bridge processes are dispersive.

KEYWORDS

Indian Ocean Dipole (IOD), El Niño and Southern Oscillations (ENSO), oceanic channel, atmospheric bridge, Indonesian Throughflow (ITF), Coupled Model Intercomparison Project phase 5 (CMIP5)

Introduction

The El Niño and the Southern Oscillations (ENSO) are the strongest large-scale ocean-atmosphere interactions on the interannual time scales over the tropical Pacific Ocean (Bjerknes, 1969; Philander, 1990). The Indian Ocean Dipole (IOD) is a zonal dipole mode of sea surface temperature anomalies (SSTA) over the tropical Indian Ocean (Saji et al., 1999; Webster et al., 1999). The Indian Ocean variability is strongly influenced

by the Pacific ENSO (e.g., Chowdary and Gnanaseelan, 2007; Du et al., 2009, 2013; Gnanaseelan et al., 2012; Zhang et al., 2021; Mukhopadhyay et al., 2022). Some studies have suggested that IOD is forced by ENSO (Alexander et al., 2002; Hastenrath, 2002; Lau and Nath, 2003; Cai et al., 2005; Stuecker et al., 2017). Some other studies suggest that IOD be an intrinsic mode of interannual variability of the coupled ocean-atmosphere climate system over the tropical Indian Ocean (Saji et al., 1999; Yamagata et al., 2003; Annamalai et al., 2005; Behera et al., 2006; Yang et al., 2015). Existing studies have suggested that IOD can feedback on the tropical Pacific SSTA evolution (e.g., Wu and Kirtman, 2004; Kug and Kang, 2006; Song et al., 2008; Xie et al., 2009; Luo et al., 2010; Nagura and McPhaden, 2014; Kajtar et al., 2015, 2017; Wang, 2019; Duan et al., 2020), the processes of which have been attributed to the atmospheric bridge (Clarke and Van Gorder, 2003; Kug et al., 2006; Izumo et al., 2010; Ohba et al., 2010; Kug and Ham, 2012; Santoso et al., 2012) or/and through the oceanic channel of the Indonesian seas (Yuan et al., 2011, 2013; Zhou et al., 2015; Zhao et al., 2016; Trenberth and Zhang, 2019). Based on numerical experiments by blocking the Indonesian gateway in a coupled climate model, Kajtar et al. (2015) suggest that the atmospheric bridge is a robust element of the Indo-Pacific interactions, albeit the IOD-ENSO relationship is weaker than when the oceanic channel is open. On the other hand, by shutting down the atmospheric bridge, numerical experiments have shown significant influence of both positive and negative IOD events on ENSO, implying the role of the oceanic channel (Yuan et al., 2011; Zhou et al., 2015; Wang et al., 2021).

The importance of the IOD-forced ENSO variability lies in the fact that this class of ENSO can be predicted beyond the spring predictability barrier if IOD is used as a precursor (Izumo et al., 2010, 2014; Yuan et al., 2011, 2013). The mechanism underlying the enhanced predictability has been attributed to the atmospheric bridge by Izumo et al. (2010): a negative IOD leads to enhanced easterly anomalies over the western Pacific Ocean in winter forcing upwelling Kelvin waves propagating eastward. The ensuing advective-reflective ocean-atmosphere coupled process generates anomalous warming in the eastern equatorial Pacific cold tongue in the next winter. Later, the forcing mechanism is updated as forced by the IOD western pole related to the Indian Ocean basin mode after the IOD subsides abruptly in winter (Izumo et al., 2016). In contrast, Yuan et al. (2011) argue that the oceanic channel, i.e., the Indonesian Throughflow (ITF) variability, should play a critical role in propagating the IOD anomalies into the equatorial Pacific Ocean. The oceanic channel dynamics have been corroborated by longer time lags of the IOD-ENSO precursory teleconnection for oceanic than atmospheric anomalies in observations (Yuan et al., 2013). They have shown that the lag correlations between sea surface temperature anomalies (SSTA) or sea surface height anomalies (SSHA) in the southeastern tropical Indian Ocean (STIO) in fall and the oceanic anomalies, i.e., SSTA, SSHA, and subsurface temperature anomalies, in the equatorial Pacific cold tongue 1-year later are all significant, suggesting that the interannual variability of the ITF play an important role in connecting the IOD with ENSO. In comparison, the lag correlations between the surface zonal wind anomalies (SZWA) over the far western equatorial Pacific (WEP) in fall and the SZWA, SSTA, and SSHA in the central and eastern equatorial Pacific in the next fall are all insignificant, suggesting that the IOD-related atmospheric bridge should not be responsible for the enhanced predictability at the 1-year time lag. The oceanic channel dynamics have been shown to be important for the skills of the climate models in simulating ENSO (Xu et al., 2013). The initial condition errors of sea temperature in the Indian Ocean are identified as causal factors of the spring predictability barrier for El Niño, with two types of errors (positive and negative IOD-like patterns) emphasize the mechanism of atmospheric bridge and oceanic channel, respectively (Zhou et al., 2019, 2020, 2021).

Both the IOD (Ashok et al., 2004; Abram et al., 2008; Ummenhofer et al., 2011) and ENSO (Gershunov and Barnett, 1998; Wang and Picaut, 2004; An et al., 2005; Leloup et al., 2007) are subjected to decadal and multi-decadal variability. Meanwhile, the ITF also shows interannual to decadal response to the Indo-Pacific forcing (Tillinger and Gordon, 2010; Li et al., 2018, 2020). Consquently, the IOD-ENSO relationship is subjected to decadal and multi-decadal variability as well (Yuan and Li, 2008; Huang et al., 2010; Xie et al., 2010; Chowdary et al., 2012; Tao et al., 2015; Sang et al., 2019). In terms of the oceanic channel dynamic, it is identified to have positive and negative phases of decadal oscillations. The IOD-ENSO precursory teleconnection in SSTA during the negative phases are suppressed by decadal deepening of the thermocline in the eastern equatorial Pacific (Xu and Yuan, 2014).

The cross-basin coupling between the tropical Indian and Pacific Oceans on the interannual time scale is reproduced well in the climate system models that involved in the phase five of the Coupled Model Intercomparison Project (CMIP5) (Ha et al., 2017). Jourdain et al. (2016) have shown robust relationship between IOD and its following ENSO in the historical simulations of the CMIP5 models, with asymmetry between negative IOD leading El Niño and positive IOD leading La Niña. Yuan et al. (2018) have shown that the IOD-ENSO precursory teleconnection tends to get stronger over the past century in the historical simulations of the CMIP5 models. The oceanic channel dynamics in the CMIP5 models, however, have not been investigated. Therefore, in this study, we will focus on the evaluation of model skills and deficiencies in simulating the oceanic channel and atmospheric bridge processes. The next section describes the observational data and the CMIP5 model experiments. Section Results compares the observed and simulated lag correlations to assess the skills of the CMIP5 coupled climate system models in simulating the oceanic channel and the atmospheric bridge. Discussions and conclusions are summarized in section Conclusions and summary.

Data and method

Observations

The observational SST data used in this study are the Hadley center SST dataset (HadISST; Rayner et al., 2003) with a horizontal resolution of 1° × 1° grid from 1871 to the present. The SSH data are the Version 5.0 of daily gridded absolute dynamic topography products produced by the Segment Sol multi-missions dALTimetrie, d'orbitographie et de localization précise/Data Unification and Altimeter Combination System (SSALTO/DUACS) and distributed by the Archiving, Validation, and Interpretation of Satellite Oceanographic (AVISO), with support from CNES (http://www.aviso.altimetry.fr/duacs/). The dataset is daily, at a resolution of 0.25° × 0.25°, which is available from October 1992 to the present (Ducet et al., 2000). The subsurface temperature data are obtained from the Quality controlled subsurface ocean temperature and salinity profiles and objective analyses (EN) dataset consists of two products: observed subsurface ocean temperature and salinity profiles with data quality information, and objective analysis formed from the profile data with uncertainty estimates (Good et al., 2013). The latest version of the data is EN.4.2.1, with a horizontal resolution of 1° × 1° and 42 vertical levels from 1900 to the present. The surface wind data are from the Twentieth Century Reanalysis V3 (20CRv3), the most recent version of the reanalysis spaning 1836 to the present, with a horizontal resolution of 1° × 1° (Slivinski et al., 2019).

CMIP5 simulations

The model outputs used in the study are the historical simulations based on the experimental design of CMIP5 (Taylor et al., 2012). The historical experiments have considered both anthropogenic and natural forcing, covering the period from the mid-19th century to the present. A total of 23 historical simulations are analyzed in this study (Supplementary Table 1). For simplicity, only one of the ensemble members (named "r1i1p1") is analyzed for each model. There is only a few CMIP5 model have provided more than 10 ensemble members. In this study, we employ the CNRM-CM5 historical simulation, which includes 10 ensemble experiments, to discuss the dispersion of the IOD-ENSO precursory teleconnection in a single climate system model.

Statistical analysis

The Niño3.4 index is defined as the averaged SSTA in the area of the equatorial central and eastern Pacific (5°S–5°N, 170°-120°W). The Dipole Mode Index (DMI) is calculated as the difference of SSTA between the western (10°S–10°N, 50°-70°E) and southeastern tropical Indian Ocean (10°S–0°, 90°-110°E) (Saji et al., 1999). The WEP wind is represented by the surface wind anomalies averaged over (5°S–5°N, 130°-150°E).

The lag correlation is calculated as the correlation between the anomalies in boreal fall and those in the following winter through fall seasons. The boreal seasons are defined as spring (March to May), summer (June to August), fall (September to November), and winter (December to the following February). The decadal variability of the IOD-ENSO teleconnection in the observed SSTA data is investigated using running mean lag correlations over time windows of 7, 11, 21, and 31 years. The IOD-ENSO teleconnection in the CMIP5 models is investigated using only the 11-year running mean lag correlations for simplicity. The Student's *t*-test is employed to determine the 95% significance level of the correlations. Throughout this paper, we call the IOD year as Year 0 and the year following it Year +1.

Results

IOD-ENSO precursory teleconnection in CMIP5 models

The IOD-ENSO precursory teleconnection, as represented by the running mean lag correlations between the STIO SSTA in fall and the Niño3.4 SSTA in the next fall, with a running window of 11, years, undergoes obvious decadal variability (Xu and Yuan, 2014). As shown in Figure 1A, the running mean lag correlations after the 1990s are positive, consistent with the analysis of Yuan et al. (2013). Evidently, the correlations in that study represent the IOD-ENSO teleconnection during a decade of positive lag correlations. It can be found that during some of the decades, e.g., the 1871–1900, the running mean lag correlations are negative, suggesting that El Niño events follow positive IOD events and La Niña events follow negative IOD events at the 1-year time lag. Thus, the teleconnection during the negative correlation periods is believed to be different from that during the positive correlation periods. The structure and possible dynamics of the teleconnection during the negative phases of the decadal variability have been analyzed in Xu and Yuan (2014). In this study, we only focus on the positive phases for two reasons. First, the oceanic channel dynamics are less effective during the negative phases. Second, the positive lag correlations are stronger and more persistent than the negative over the past 150 years.

The CMIP5 model simulations are subject to the inherent oscillations of the coupled climate system models so that their simulated IOD and ENSO generally do not match with the timing in nature (Taylor et al., 2012). As a result, the running mean lag correlations in CMIP5 historical simulations

10.3389/fclim.2022.996343

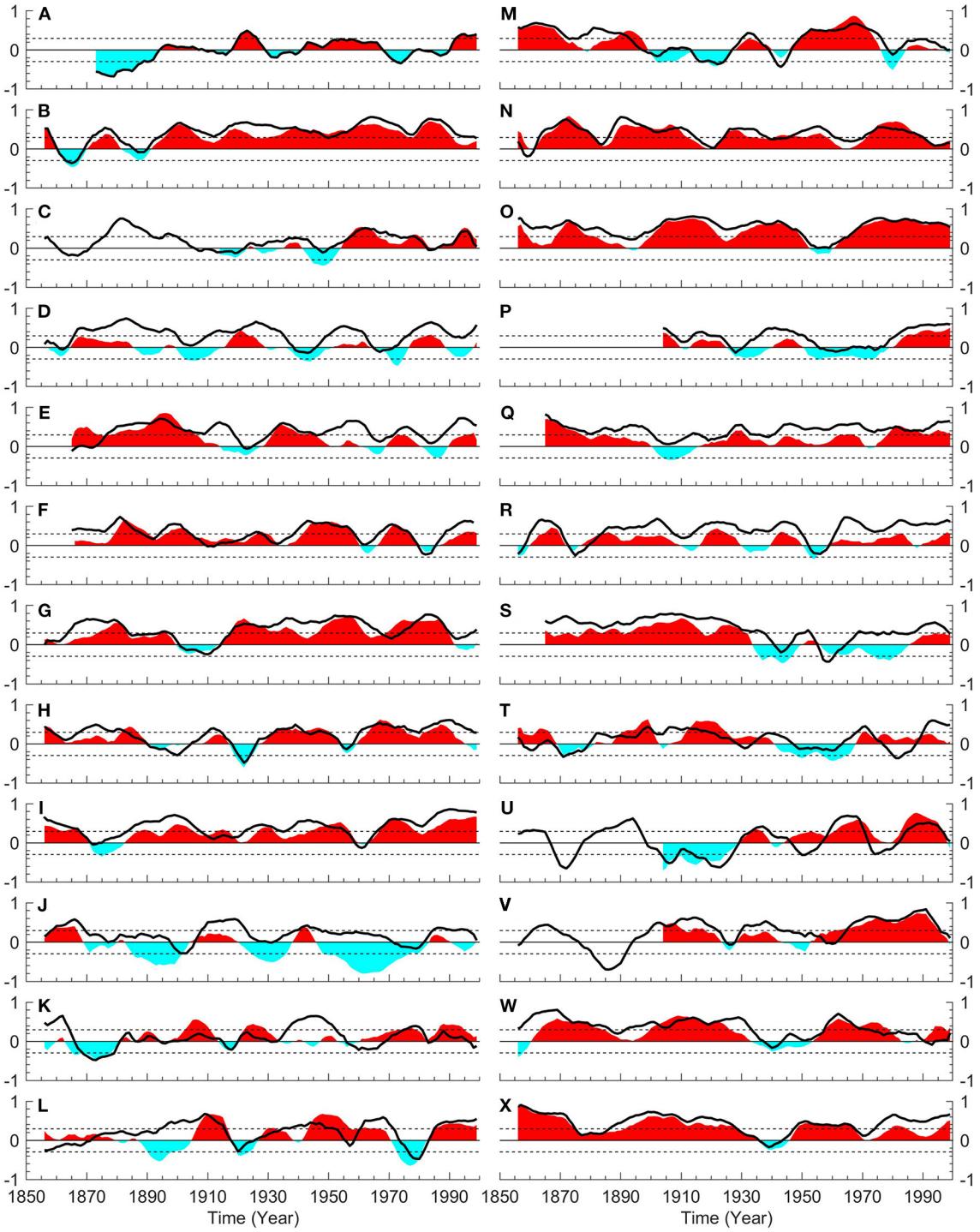

FIGURE 1
Lag correlation between the STIO SSTA (SSHA) in fall and the SSTA (SSHA) in the Niño3.4 area in the next fall with a running window of 11 years in HadISST and CMIP5 historical simulations, the horizontal axis showing window central date. Shading and curves indicate correlation of SSTA and SSHA, respectively. Index **(A–X)** refers to different CMIP5 model as listed in Supplementary Table 1.

do not necessarily match the phase of the decadal variability in the observed SST data. Nevertheless, all of the running lag correlations of the CMIP5 model simulations have shown the same kind of decadal variability of the IOD-ENSO teleconnection as in the observation (Figure 1). The running mean lag correlations between the STIO SSHA in fall and the

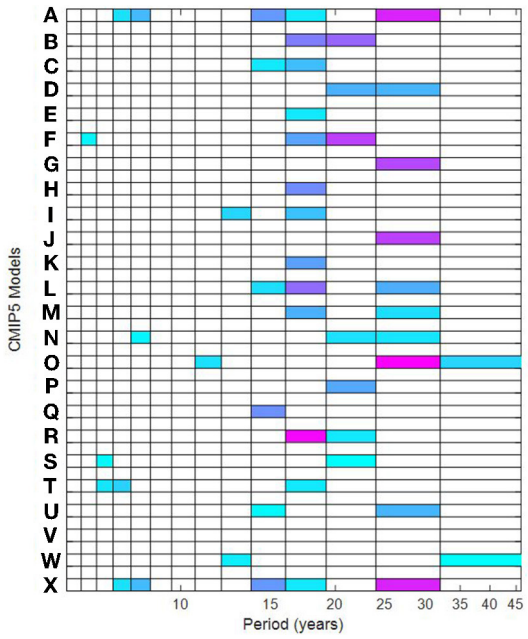

FIGURE 2
Power spectrum density (PSD) of the 11-year running mean lag correlation between STIO SSTA in fall and Niño3.4 SSTA in the next fall in HadISST and CMIP5 simulations. Only PSD above the 95% significance level are shaded. Index **(A–X)** refers to different CMIP5 model as listed in Supplementary Table 1.

Niño3.4 SSHA in the next fall have also shown the same decadal variability associated to that of SSTA lag correlations, but with the positive correlations of SSHA much higher than those of SSTA in the CMIP5 historical simulations, an effect perhaps due to the imperfect correlation between the upwelling anomalies and the SSTA.

The power spectra of the running mean lag correlations indicate one or two significant periods from 15 to 50 years, suggesting that some kinds of decadal-to-multidecadal variability of the IOD-ENSO teleconnection have been simulated successfully by the CMIP5 models (Figure 2). In the following context of this paper, the results of the CMIP5 simulations during the periods when the running mean lag correlations are positive and above one standard deviation are used to represent the positive phases of the decadal variability. The time series of these periods are *Z*-score standardized and concatenated into a long time series, the lag correlations of which are analyzed and compared with those in the observations to assess the skills of the CMIP5 models in simulating the IOD-ENSO teleconnection and to study the dynamics of the teleconnection.

The phase-locking of the IOD peak to the boreal fall season has been simulated well in the CMIP5 climate models (Zheng et al., 2013; Liu et al., 2014). The cross-model-averaged lag correlations between the STIO SSTA in fall and the tropical Indo-Pacific SSTA in the following winter through fall during the positive phases of the decadal variability of the 23 CMIP5 historical simulations are compared with those in HadISST (Figure 3). The observed lag correlations show significant IOD- and ENSO-type teleconnections, above the 95% significance level, with positive correlations in the eastern tropical Indian and western Pacific Oceans and negative correlations in the eastern equatorial Pacific cold tongue in the winter of Year 0 (Figure 3A). The significant correlations disappear in the equatorial Pacific cold tongue in the spring of Year +1, suggesting that the atmospheric bridge processes giving rise to the IOD- and ENSO-type teleconnections in winter are short lived and have not lasted through the spring season, consistent with the existence of the spring barrier (Figure 3B). The significant lag correlations above the 95% significance level, re-emerge in summer and fall of Year +1 (Figures 3C,D), with a similar pattern of the IOD-ENSO lag teleconnection as in the winter of Year 0, except for an opposite sign. These results are consistent with those of Yuan et al. (2013), suggesting that the use of IOD anomalies as precursors provides potential for improved ENSO predictions beyond the spring predictability barrier during the positive phases of the decadal oscillation. The lag correlations of the SSTA in the CMIP5 historical simulations show similar pattern and evolution in the equatorial Pacific (Figures 3E–H), which are negative in the central-eastern equatorial Pacific in the winter of Year 0 but positive in the summer and fall of Year +1. The lag correlations in the cold tongue in spring are vanishingly small, suggesting the effects of the spring barrier.

Figure 4 shows the numbers of CMIP5 models with significant positive lag correlations of SSTA between the STIO and the tropical Indo-Pacific Ocean in the following winter through fall seasons. Since the oceanic channel dynamics are associated with the eastward movement of significant positive correlations, the numbers of CMIP5 models for negative lag correlations are not shown here. It shows that around half of the CMIP5 models have simulated the ENSO-type teleconnection and its disappearance in the STIO and the western tropical Pacific (Figures 4A,B). In the CMIP5 historical simulations, more than half have reproduce the re-emergence of significant positive correlations in the central-eastern Pacific Ocean in summer of Year +1 (Figure 4C). Almost all of the CMIP5 historical simulations have produced the significant positive correlations in the central-eastern Pacific Ocean in summer of Year +1. In around 16 (summer of Year +1) and 6 (fall of Year +1) of the CMIP5 models, the lag correlations of the SSTA in the equatorial Pacific cold tongue are still significant, above the 95% significance level, even if the signals associated with Niño3.4 index are regressed out from the cold tongue SSTA, suggesting independence of the IOD-ENSO precursory

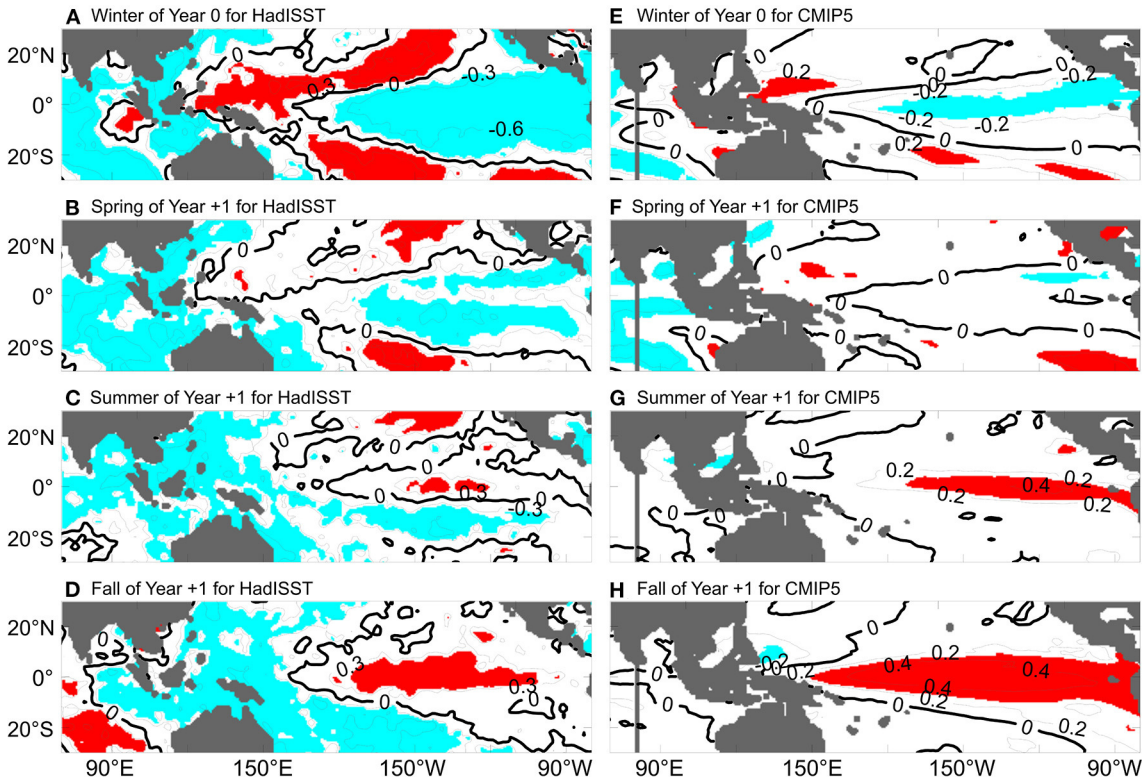

FIGURE 3
Lag correlations between the STIO SSTA in the fall of Year 0 and the tropical Indo-Pacific SSTA from the winter of Year 0 through the fall of Year +1. **(A–D)** HadISST; **(E–H)** cross-model averaged from CMIP5 historical simulations. The red and blue shading indicate the 95% significance level of positive and negative correlations, respectively.

teleconnection from ENSO in these CMIP5 climate models (Figures 4G,H).

Lag correlations associated with oceanic channel dynamics

The lag correlations of SSTA are closely related to the so-called oceanic channel dynamic, which are evidenced by the lag correlations of SSHA and subsurface temperature anomalies. The lag correlations between the STIO SSHA in fall and the SSHA in the tropical Indian and Pacific Oceans in the following winter through fall in the altimeter data of 1993–2012 and averaged from the CMIP5 historical simulations are shown in Figure 5. The altimeter SSHA lag correlations in the winter of Year 0 have shown the typical IOD- and ENSO-type teleconnection over the tropical Indo-Pacific Ocean (Figure 5A), which is reminiscent of the SSTA lag correlations. The significant lag correlations of SSHA persist in the western equatorial Pacific Ocean and in the Indonesian Seas in the spring of Year +1, in contrast to the vanishing lag correlations of SSTA in the equatorial Pacific Ocean. A belt of positive significant lag correlations extends to the eastern equatorial Pacific, suggesting the propagation of the equatorial Kelvin waves (Figure 5B), which lead to the significant positive lag correlations in the central and eastern equatorial Pacific cold tongue in the summer and fall of Year +1 (Figures 5C,D). All these characteristics and the dynamics associated with them have been discussed in detail in Yuan et al. (2013). The eastward movement of the significant lag correlations of SSHA from the winter of Year 0 through the fall of Year +1 suggests strongly that the oceanic channel, i.e., the interannual variability of the ITF, play an important role in the IOD forcing on the equatorial Pacific ENSO at the time lag of 1 year. The CMIP5 historical simulations have reproduced weaker average SSHA lag correlations in the cold tongue in the winter of Year 0 (Figure 5E) than in the observational analysis. This difference can be explained by the fact that the simulated ENSO phase-locking with the seasonal cycle ranges from fall to winter in the cold tongue in different models (Bellenger et al., 2014; Ham and Kug, 2014). The eastward movement of significant positive lag correlations of SSHA from the winter of Year 0 to the fall of Year +1 has been simulated successfully by the CMIP5 models on average (Figures 5E–H).

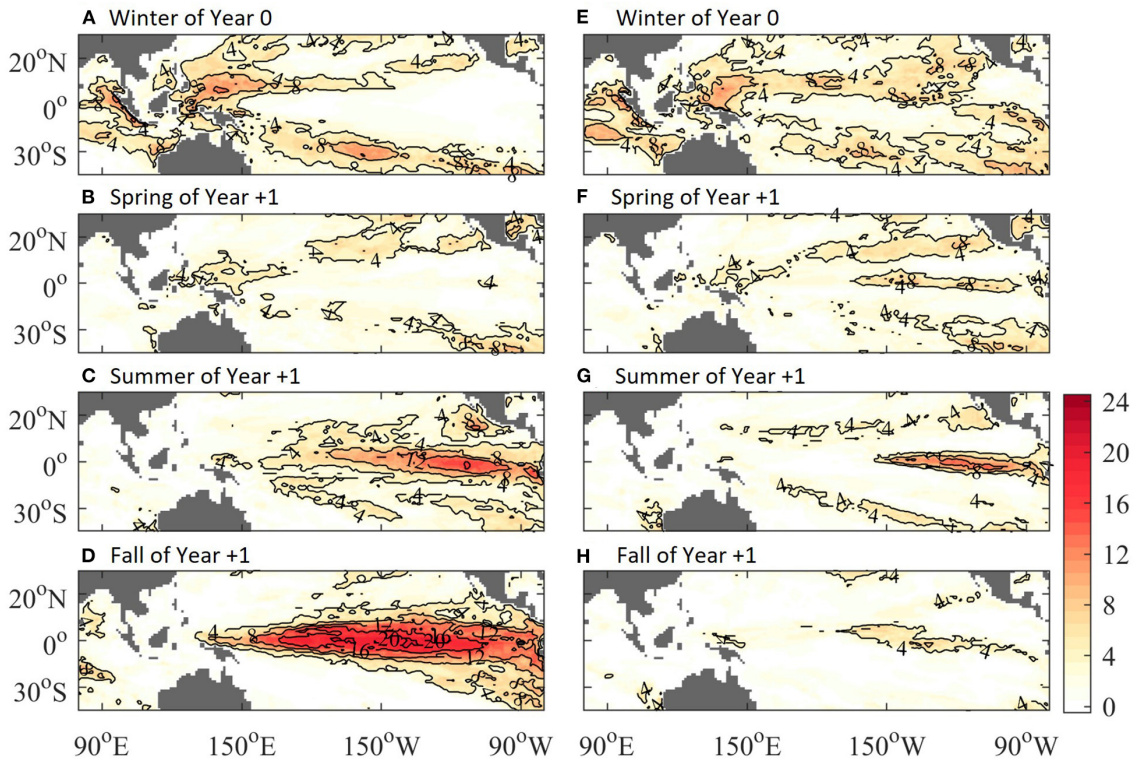

FIGURE 4
Numbers of CMIP5 models with significant positive correlations between the STIO SSTA in fall and the tropical Indo-Pacific Oceans SSTA in **(A)** winter of Year +0, **(B)** spring of Year +1, **(C)** summer of Year +1, and **(D)** fall of Year +1. **(E–H)** are same as **(A–D)**, but with the ENSO signal removed.

The SSHA lag correlations in the fall winter through fall seasons show good consistency in the CMIP5 historical simulations (Figures 6A–D), in good agreement with those in observation (Figure 5). The significant correlations still exist in more than half of the CMIP5 models in the STIO and western equatorial Pacific in the winter of Year 0, and spring of Year +1, and in the central-eastern equatorial Pacific in the summer and fall of Year +1, with the ENSO signal removed (Figures 6E–H). These results suggest that the oceanic channel dynamics, which are responsible for the IOD-ENSO precursory teleconnection, have been included in most of the CMIP5 climate models. It should be noting that few of the CMIP5 models have produced artificially correlations at 1-year time lag for both SSTA and SSHA, suggesting model deficiency (Supplementary Figures A1,A2). For example, the MIROC5 fails to reproduce the significant positive lag correlation of SSTA; the MPI-ESM-LR and MPI-ESM-P fail to reproduce the significant positive lag correlation of SSHA; and the HadGIM2-ES produces highly significant positive correlations of SSHA over the entire tropical Indo-Pacific Ocean.

The lag correlations between the STIO SSTA in fall and the subsurface temperature anomalies in the vertical section along the equatorial Pacific Ocean from the winter of Year 0 through the fall of Year +1 suggest eastward propagation of the IOD anomalies from the Indian Ocean to the equatorial Pacific Ocean through the Indonesian seas in the thermocline (Figures 7A–D). After reaching the equatorial Pacific, the IOD induced signal is amplified by the air-sea coupling over the tropical Pacific, thereby resulting in the persistent significant positive correlations in the cold tongue through summer to fall of Year +1 (Yuan et al., 2011). The lag correlations outcrop in the central and eastern equatorial Pacific in the summer and fall of Year +1 to impact the SSTA in the cold tongue in the observations (Figure 7D). This eastward movement of positive lag correlations, above the 95% significance level in the thermocline of the equatorial Pacific Ocean is reproduced well on average by the historical simulations of CMIP5 climate models (Figures 7E–H). The propagation together with the SSHA lag correlations suggest the importance of the oceanic channel dynamics, i.e., the variability of ITF transport, in the forcing of the oceanic anomalies in the equatorial Pacific Ocean by the Indian Ocean (Yuan et al., 2013).

The lag correlations of subsurface temperature anomalies tend to propagate faster in the CMIP5 models than those in the observation, as revealed by the significant correlations reach as far as 120°-150°W in more than 12 of the CMIP5 models

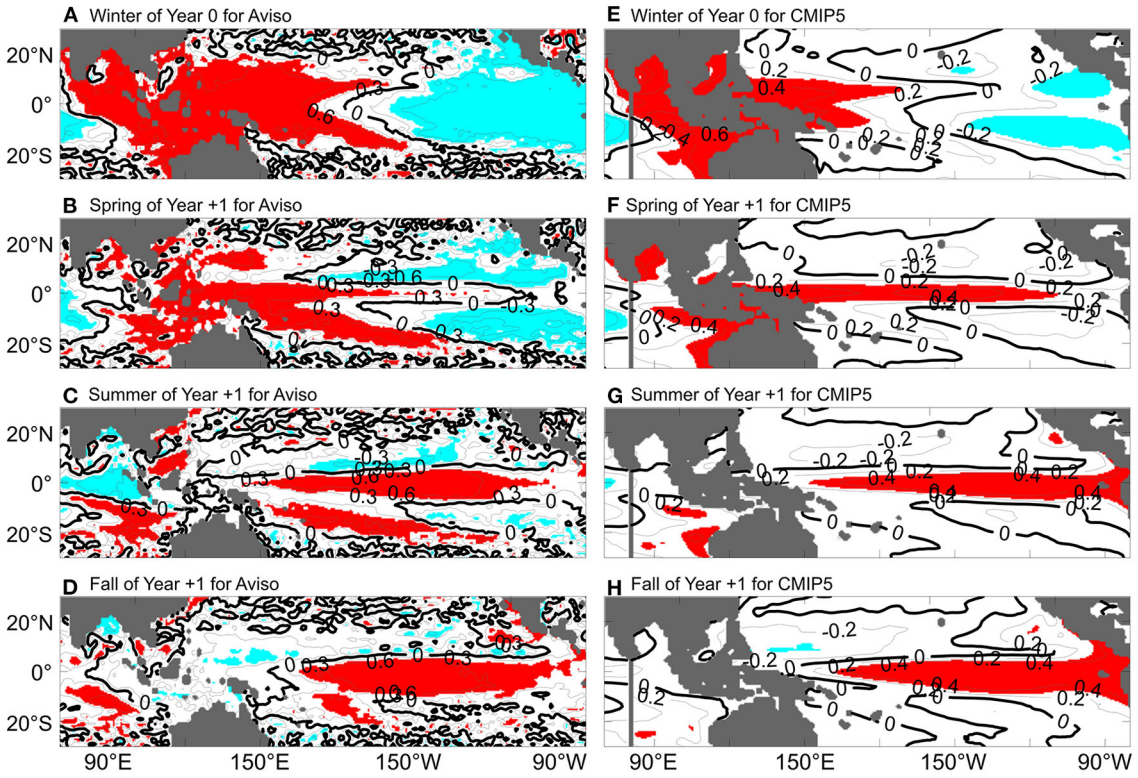

FIGURE 5
Lag correlations between the STIO SSHA in the fall of Year 0 and the tropical Indo-Pacific SSHA from the winter of Year 0 through the fall of Year +1 during positive phases. **(A–D)** Aviso. **(E–H)** cross-model averaged from CMIP5 historical simulations. The red and blue shading indicate the 95% significance level of positive and negative correlations, respectively.

in spring of Year +1, and surfaces in the cold tongue in summer of Year +1, roughly lead the observation by 3 months (Figures 8A–C). In addition, the significant lag correlations in fall of Year +1 are of broader and deeper extension in the CMIP5 models (Figure 8D), which may be attributed to deeper thermocline and/or less diffusion in these models (Castaño-Tierno et al., 2018). In more than half of the CMIP5 models, the eastward propagation of significant positive correlations persists in the subsurface temperature anomalies, even if the ENSO signal is removed (Figures 8E–H). Overall, the subsurface lag correlations corroborate with those of SSTA and SSHA, suggesting robust oceanic channel dynamics are included in the CMIP5 climate models.

Lag correlations associated with atmospheric bridge processes

The lag correlations between the surface zonal wind anomalies (SZWA) over the WEP in fall and the tropical Indo-Pacific SZWA, SSTA and SSHA in the next fall have been used to diagnose the atmospheric bridge processes over the tropical Indo-Pacific Ocean (Xu et al., 2013; Yuan et al., 2013). These correlations are calculated in the CMIP5 historical simulations and are shown in Figures 9, 10, respectively. As suggested by Yuan et al. (2013), the atmospheric bridge processes should be short lived, and thus cannot responsible to the IOD-ENSO precursory teleconnection at 1 year time lag, which is evidenced by insignificant correlation of WEP SZWA with SSTA and SSHA in the cold tongue area. In the CMIP5 historical simulations, the atmospheric bridge related lag correlations are much dispersive, showing significant positive correlations in the cold tongue at 1 year time lag in some of the models, whereas significant negative or insignificant correlations in others.

The lag correlations between the WEP SZWA in fall and the tropical Indo-Pacific SSTA in the next fall are very dispersive, with significant positive correlations in CCSM4 and FGOALS-g2 historical simulations but significant negative correlations in CanESM2 and IPSL-CM5B-LR historical simulations in the equatorial Pacific cold tongue (Figure 9). The lag correlations between the WEP SZWA in fall and the tropical Indo-Pacific SSHA have shown similar

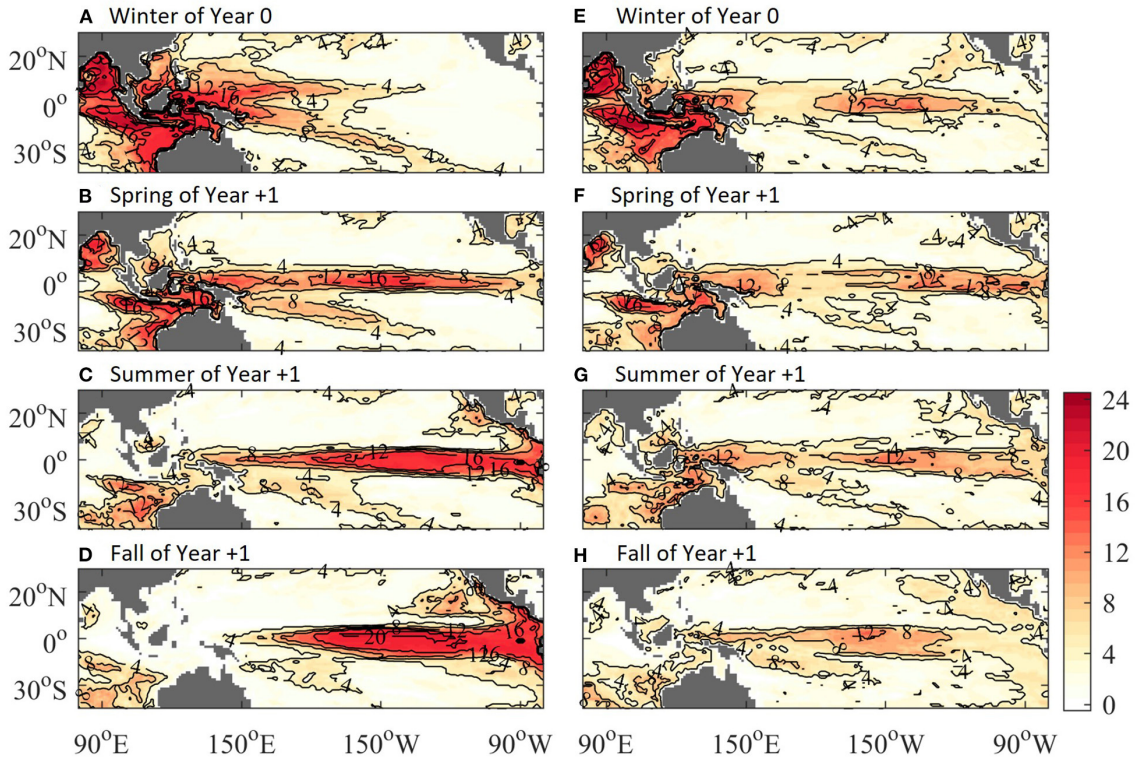

FIGURE 6
Numbers of CMIP5 models with significant positive correlations between the STIO SSHA in fall and the tropical Indo-Pacific Oceans SSHA in **(A)** winter of Year +0, **(B)** spring of Year +1, **(C)** summer of Year +1, and **(D)** fall of Year +1. **(E–H)** are same as **(A–D)**, but with the ENSO signal removed.

disparity among the different CMIP5 historical simulations (Figure 10). Sometimes, the lag correlations in Figures 9, 10 are consistent with each other. For example, in the FGOALS-g2 historical simulation, the lag correlations are all significantly positive (Figures 9P, 10P). Sometimes they are significantly different from each other. For instance, in CNRM-CM5, they are significantly negative for the SSTA correlations (Figure 9R) and positive for the SSHA correlations (Figure 10R). All of the above are significantly different from the observational analysis.

In summary, compared with the observational analysis, the lag correlations between the WEP SZWA in fall and the tropical Indo-Pacific SSTA and SSHA in the next fall in most of the CMIP5 historical simulations are unrealistic. The artificial atmospheric bridge processes in these models suggest that the atmospheric bridge is highly variable and difficulty to simulate. They are unlikely playing a dominant role in the Indo-Pacific teleconnection at the time lag beyond a season or so. The comparisons also suggest significant deficiencies in the CMIP5 models, which are harmful to the simulation and prediction of ENSO using these models.

Ensemble dispersion of the IOD-ENSO precursory teleconnection

To illustrate the ensemble dispersion of the IOD-ENSO precursory teleconnection in a single climate system model, we calculate the lag correlations in the 10 ensemble members of the CNRM-CM5 climate model. Figure 11 shows the 11-year running mean lag correlation between the STIO SSTA/SSHA in fall of Year 0 and the Niño3.4 SSTA/SSHA in fall of Year +1. The simulated IOD-ENSO precursory teleconnection shows positive correlations during most of the period from 1850 to 2005 in all of the ensemble members, suggesting consistent stronger oceanic channel dynamics in the CNRM-CM5 climate system model. In eight of the ensemble members, there are one dominant peak above the 95% significance level in the power spectral, with typical period of 15–40 years, except the r3i1pi and r10i1p1, in which show no significant peak and double peak at periods of 15–20 and 25–50 years, respectively.

During the positive phases of the decadal variability, the lag correlations between the STIO SSTA and the Indo-Pacific SSTA show good consistency among the 10 ensemble

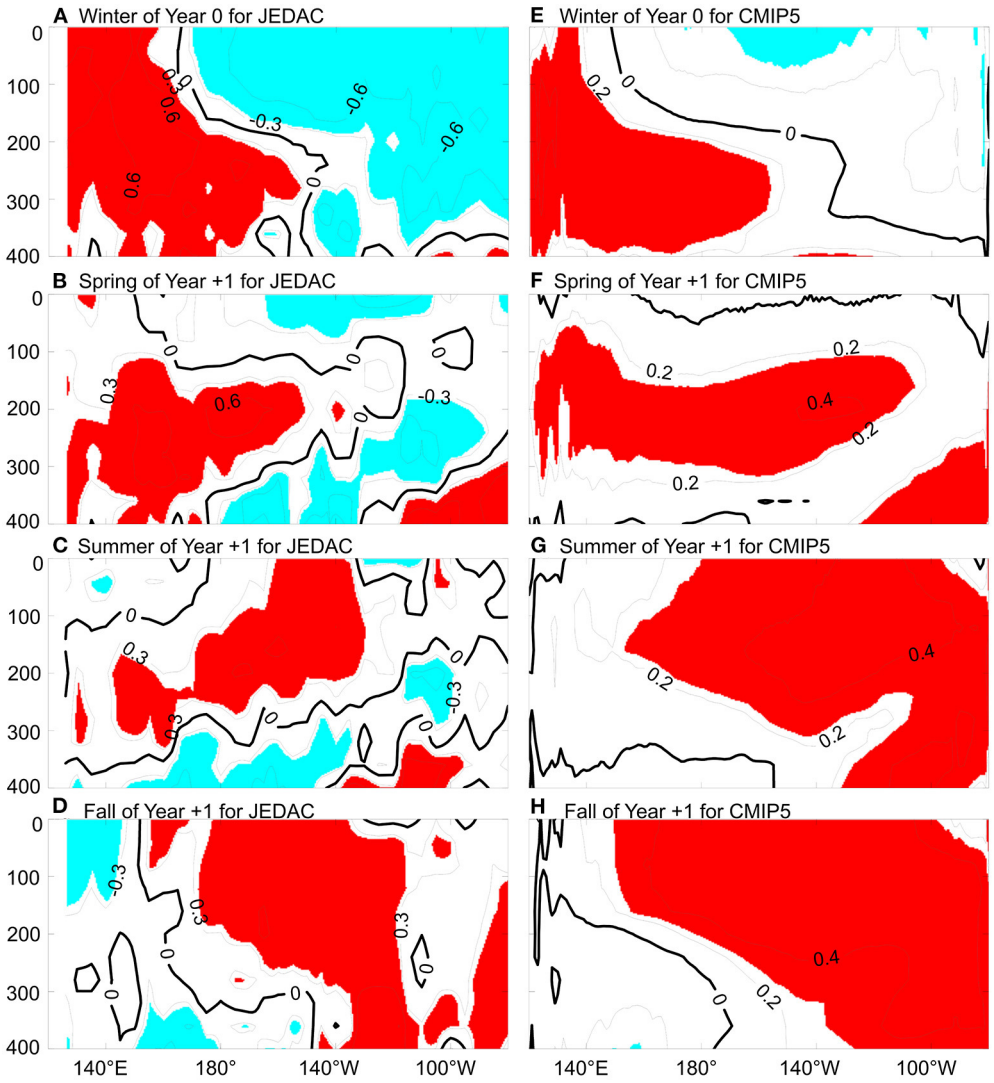

FIGURE 7
Lag correlations between the STIO SSTA in the fall of Year 0 and the subsurface temperature anomalies in the vertical section along the equatorial Pacific from the winter of Year 0 through the fall of Year +1 during positive phases. **(A–D)** JEDAC. **(E–H)** cross-model averaged from CMIP5 historical simulations. The red and blue shading indicate the 95% significance level of positive and negative correlations, respectively.

members, as revealed by the fact that all of them have produced the IOD- and ENSO-type teleconnections in winter of Year 0, and re-emerged in the central-eastern Pacific in summer and fall of Year +1 (Figure 12). The lag correlations of SSHA corroborate with those of SSTA, showing eastward propagation of significant positive correlations from the winter of Year 0 to the fall of Year +1 in all of the 10 ensemble members (Figure 13). These results suggest that the oceanic channel dynamics are consistently robust in the CNRM-CM5 climate models.

In contrast, the lag correlation associated with the atmospheric bridge processes are not consistent among the 10 ensemble members in the CNRM-CM5 climate model. The discrepancy occurs in the lag correlation between the WEP SZWA and the Indo-Pacific SSTA at the time lag of 1 year, with six ensemble members producing significant negative correlations span over the entire equatorial Pacific, two ensemble members producing significant negative correlations in limited within 150°-120°W, and two ensemble members without significant correlations (Figure 14). In all of the ensemble members, there are artificially eastward/westward propagation of significant correlations along the equatorial/off-equatorial Pacific (Figure 15). The propagation of the significant correlation between the WEP SZWA and the Indo-Pacific

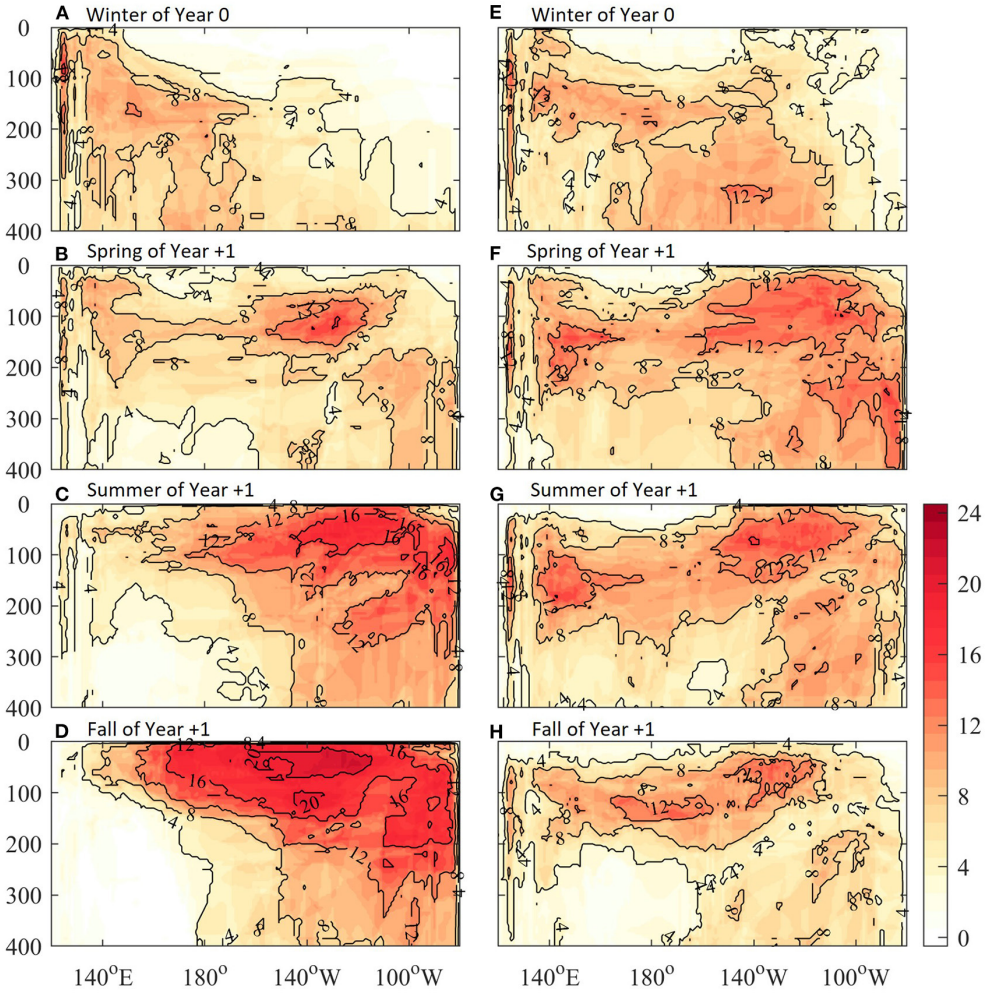

FIGURE 8
Numbers of CMIP5 models with significant positive correlations between the STIO SSTA in fall and the subsurface temperature anomalies in the vertical section along the equatorial Pacific in **(A)** winter of Year +0, **(B)** spring of Year +1, **(C)** summer of Year +1, and **(D)** fall of Year +1. **(E–H)** are same as **(A–D)**, but with the ENSO signal removed.

SSHA may attribute to the overestimated atmospheric bridge processes, thereby making the atmospheric signals longer lived in the coupled system, which are contradictory to the observation. The detailed distributions of the lag correlations associated with oceanic channel dynamics and atmospheric bridge processes can be found in the Supplementary Figures 4–8.

Conclusions and summary

In this study, the decadal variabilities of the IOD-ENSO teleconnection across the Indo-Pacific Ocean are studied based on running mean lag correlations between the SSTA or SSHA in the STIO in fall and the cold tongue SSTA or SSHA at the 1-year time lag. The analyses have shown decadal variability of the running lag correlations, with positive lag correlations generally of larger values and longer durations and the negative correlations of smaller value and shorter durations. The dynamics of the IOD-ENSO teleconnection during the positive correlation phases of the decadal oscillation are investigated using the historical simulations of the CMIP5 climate system models. The skills of the CMIP5 climate models in simulating the IOD-ENSO teleconnection at the 1-year time lag during the positive phases of the decadal variability are assessed based on the comparisons of the simulated and observed lag correlations.

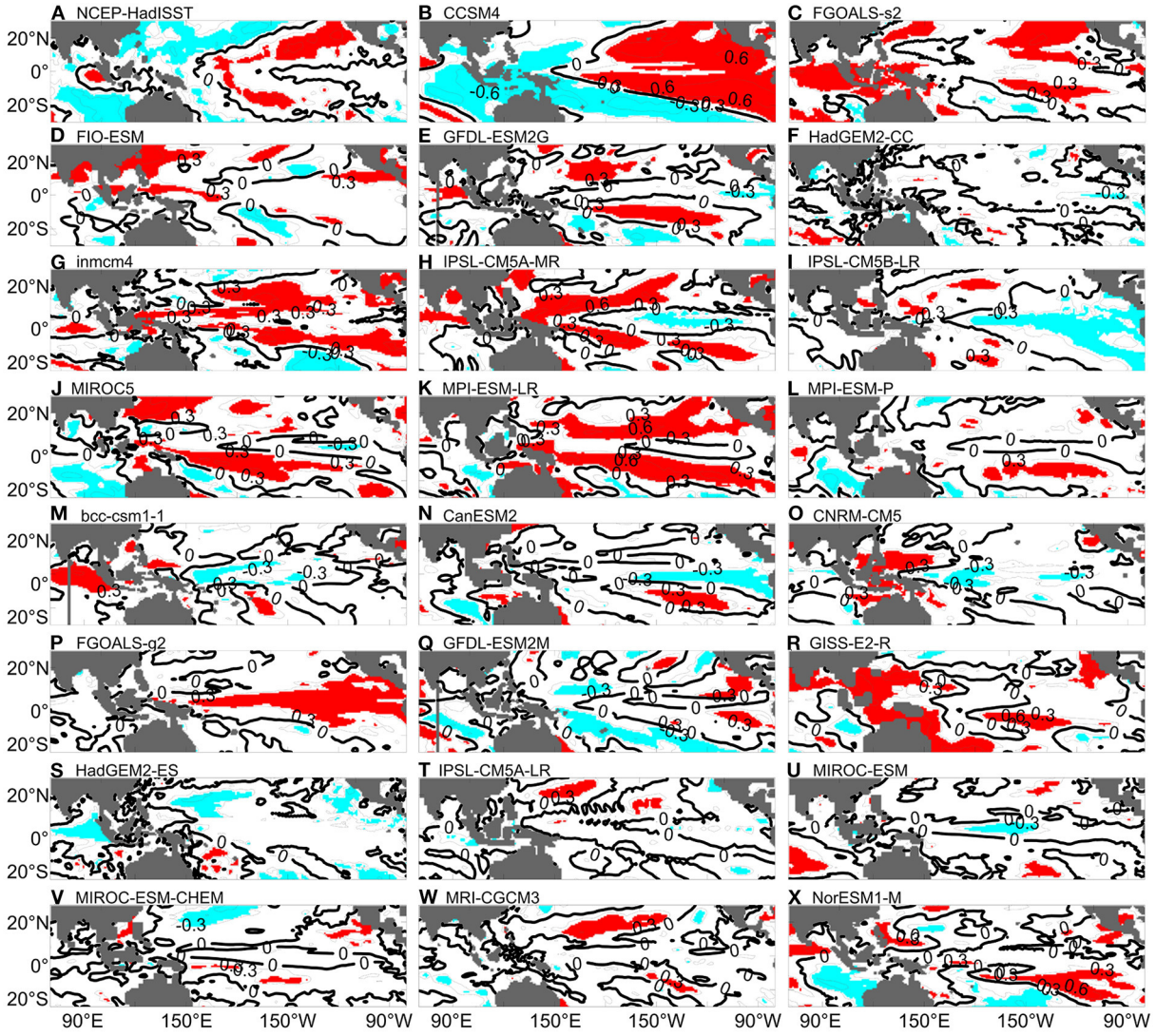

FIGURE 9
Composite lag correlations between the WEP SZWA in the fall of Year 0 and tropical Indo-Pacific SSTA in the fall of Year +1 in NCEP/HadISST and CMIP5 historical simulations during positive phases. The red and blue shading indicate the 95% significance level of positive and negative correlations, respectively. Index **(A–X)** refers to different CMIP5 model as listed in Supplementary Table 1.

The lag correlations in the CMIP5 model simulations between the STIO SSTA in fall and the Niño3.4 SSTA in the next fall show similar decadal variability as in the observational analyses, suggesting the ability of the models in simulating the decadal variability of the IOD-ENSO teleconnection in nature. During the positive phases of the decadal variability, the lag correlations between the SSTA in STIO in fall and the SSTA in the equatorial Pacific cold tongue in the next fall show positive correlations, above the 95% significance level, in most of the CMIP5 historical runs, consistent with the observational analysis. The comparisons suggest that the CMIP5 climate models are capable of reproducing the IOD-ENSO teleconnection at the 1-year time lag during the positive phases of the decadal variability. The propagation of sea level anomalies from the STIO to the central and eastern equatorial Pacific in the CMIP5 simulations are evidenced by the eastward movement of the significant positive lag correlations of SSHA between the STIO in fall and the equatorial Pacific in the subsequent seasons in CMIP5 historical simulation on average, suggesting the oceanic channel dynamics at work. The CMIP5 climate models have also simulated successfully the significant positive lag correlations between the STIO SSTA in fall and the subsurface temperature anomalies in the following year

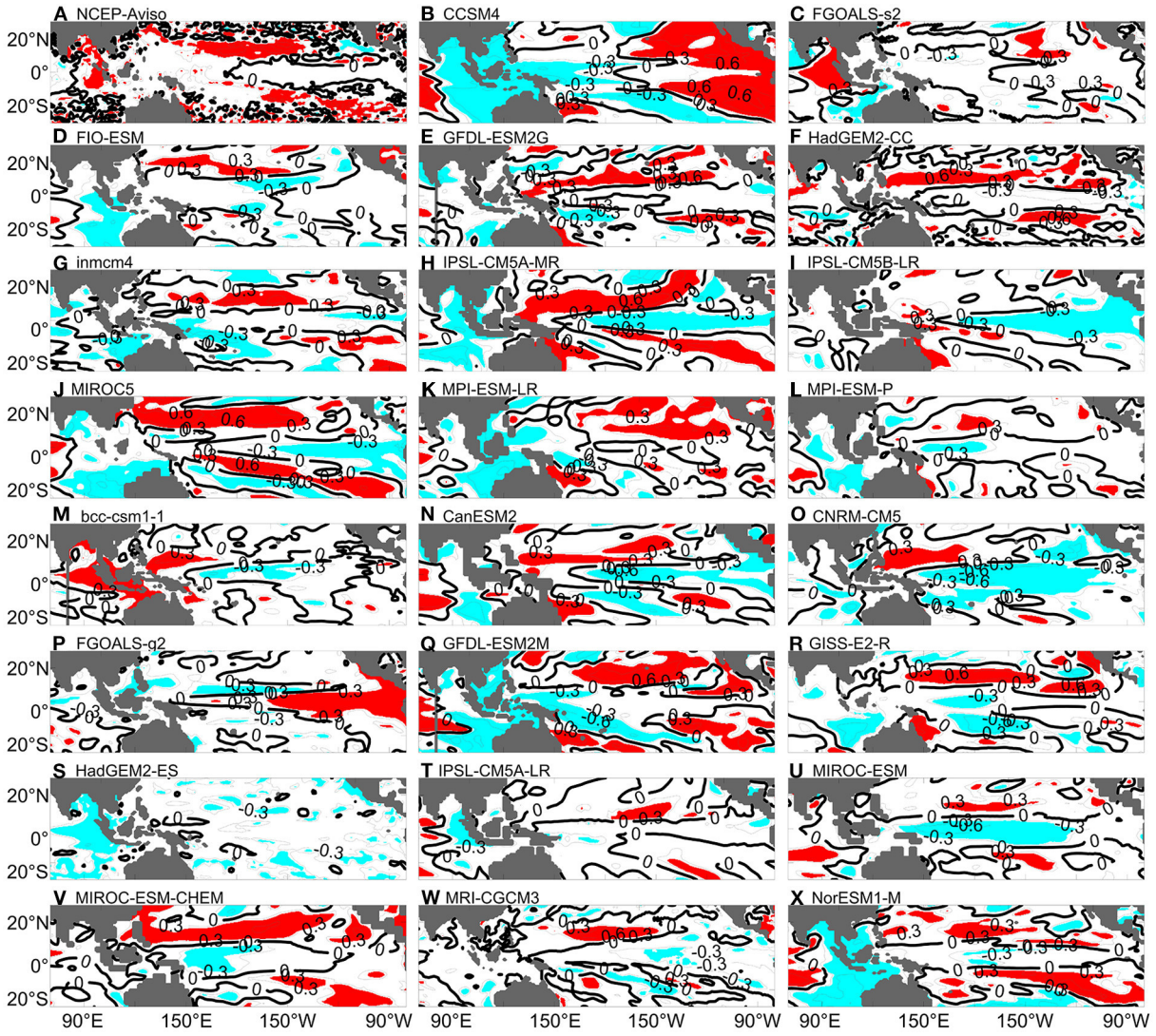

FIGURE 10
Composite lag correlations between the WEP SZWA in the fall of Year 0 and tropical Indo-Pacific SSHA in the fall of Year +1 in NCEP/Aviso and CMIP5 historical simulations during positive phases. The red and blue shading indicate the 95% significance level of positive and negative correlations, respectively. Index **(A–X)** refers to different CMIP5 model as listed in Supplementary Table 1.

moving eastward from the western Pacific to the eastern Pacific cold tongue, providing evidence of the oceanic thermocline processes in connecting IOD with ENSO at the 1-year time lag. In comparison with the observations, the simulated lag correlations in the subsurface are deeper and stronger than in the observations, probably due to a deeper thermocline in the CMIP5 model simulations. The lag correlation analyses of the oceanic anomalies of the tropical Indian and Pacific oceans suggest that most of the CMIP5 climate models have simulated the oceanic channel dynamics of the IOD-ENSO teleconnection successfully during the positive phases of the decadal variability.

In contrast, the lag correlations between the far western equatorial Pacific SZWA in fall and the tropical Indo-Pacific SZWA, SSTA, and SSHA in the following fall are found to be much dispersed among the CMIP5 climate models during the positive phases of the decadal variability. Many CMIP5 models have produced artificial atmospheric bridge processes across the Indo-Pacific Ocean in comparison with observational analyses, suggesting model deficiencies.

In a single climate system model, e.g., the CNRM-CM5, it also exists the consistency and discrepancy of lag correlations associated with oceanic channel dynamics and atmospheric

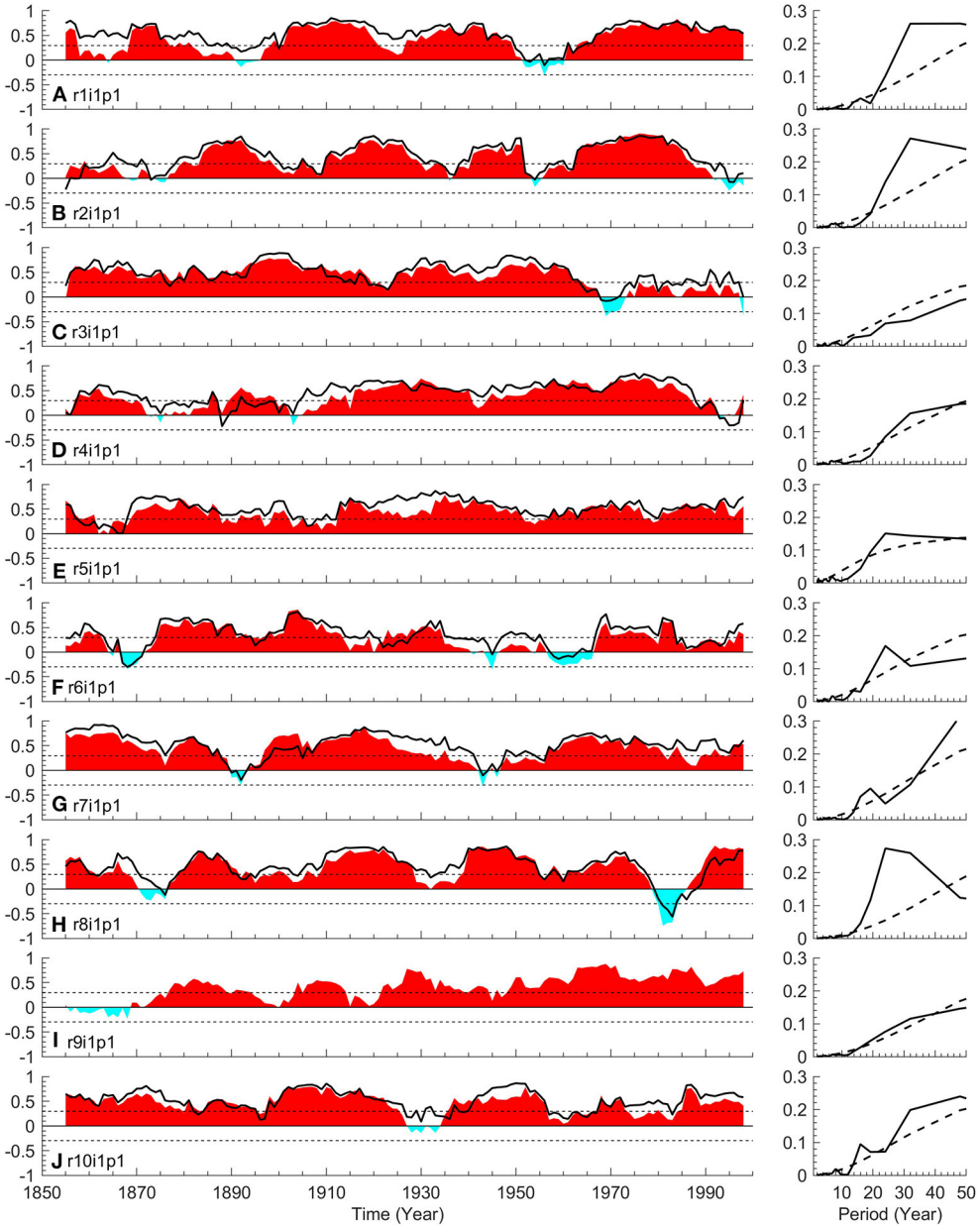

FIGURE 11
Lag correlation between the STIO SSTA/SSHA in fall and the SSTA/SSHA in the Niño3.4 area in the following fall with a running window of 11 years in different ensemble members in the CNRM-CM5 historical simulations. Shading and curves indicate correlation of SSTA and SSHA, respectively. The horizontal axis shows window central date. **(Right panels)** show corresponding power spectral of each ensemble members, dashed lines indicate the 95% significance level of the power spectra density.

bridge processes, respectively. It is worth mentioning that more analyses by employing other CMIP5 models would better reveal the ensemble dispersion of the IOD-ENSO precursory relationship. Nevertheless, it is sufficient to conclude that there exists discrepancy of simulated atmospheric bridge processes in a single climate system model. Meanwhile, although we have not gone through all ensemble members of all CMIP5 models, the consistency of oceanic channel dynamics is still robust, since all of the analyzed CMIP5 historical simulations have represent appropriate lag correlations that associated with oceanic channel dynamics, in agreement with the observations.

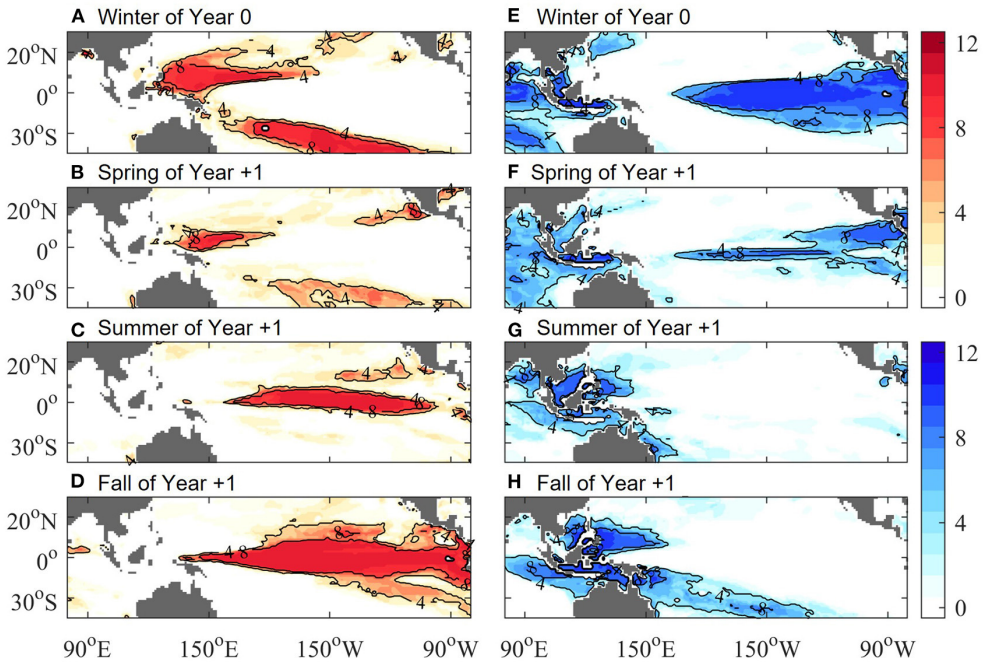

FIGURE 12
Numbers of ensemble members of the CNRM-CM5 model with significant positive correlations between the STIO SSTA in fall and the tropical Indo-Pacific Oceans SSTA in **(A)** winter of Year +0, **(B)** spring of Year +1, **(C)** summer of Year +1, and **(D)** fall of Year +1. **(E–H)** are same as **(A–D)**, but for significant negative correlations.

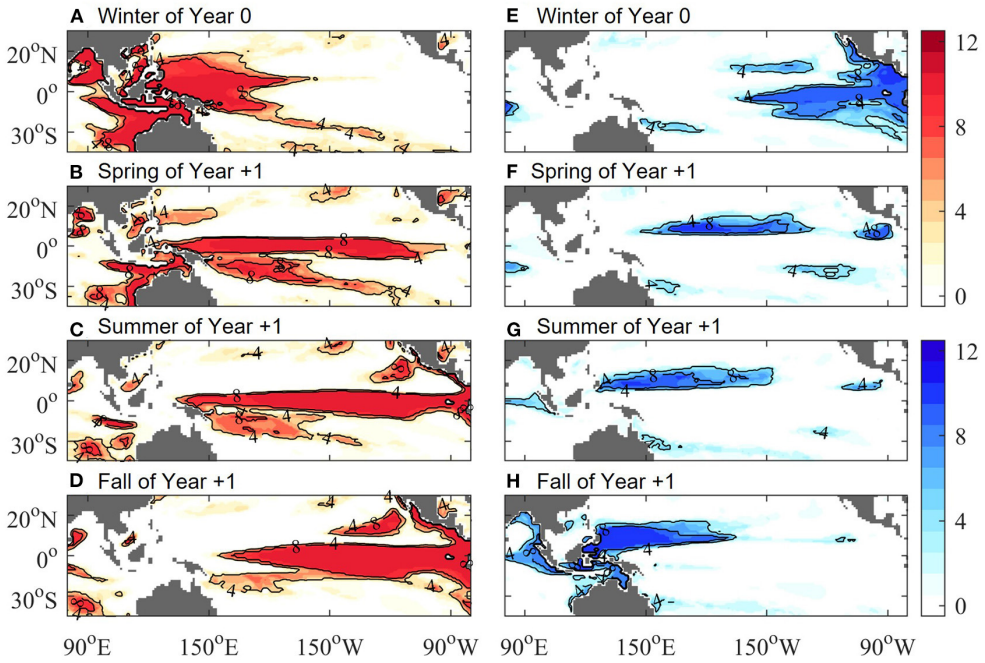

FIGURE 13
Numbers of ensemble members of the CNRM-CM5 model with significant positive correlations between the STIO SSHA in fall and the tropical Indo-Pacific Oceans SSHA in **(A)** winter of Year +0, **(B)** spring of Year +1, **(C)** summer of Year +1, and **(D)** fall of Year +1. **(E–H)** are same as **(A–D)**, but for significant negative correlations.

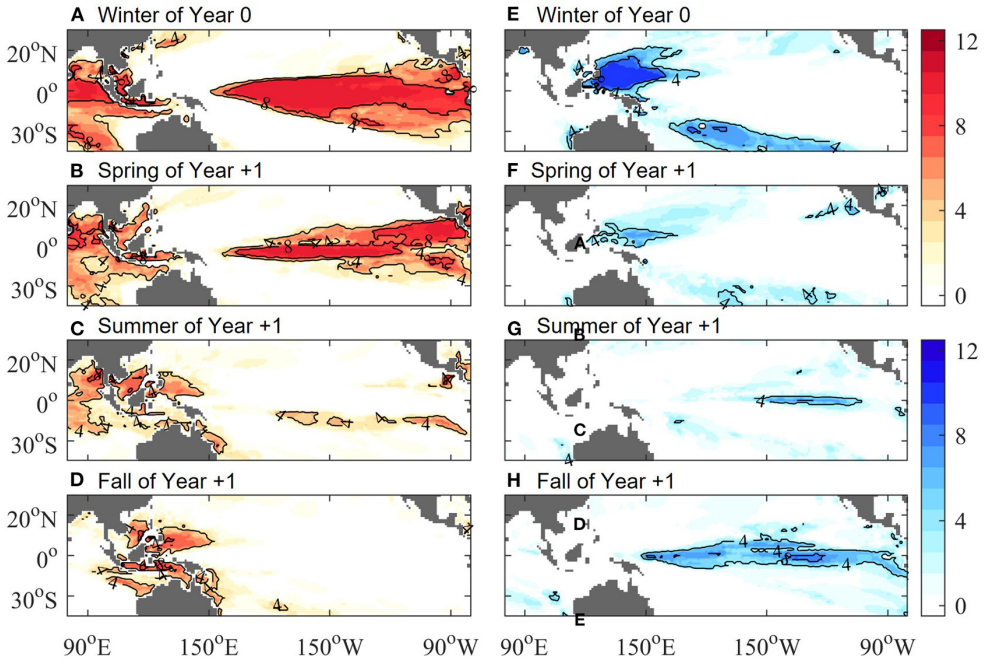

FIGURE 14
Numbers of ensemble members of the CNRM-CM5 model with significant positive correlations between the WEP SZWA in fall and the tropical Indo-Pacific Oceans SSTA in **(A)** winter of Year +0, **(B)** spring of Year +1, **(C)** summer of Year +1, and **(D)** fall of Year +1. **(E–H)** are same as **(A–D)**, but for significant negative correlations.

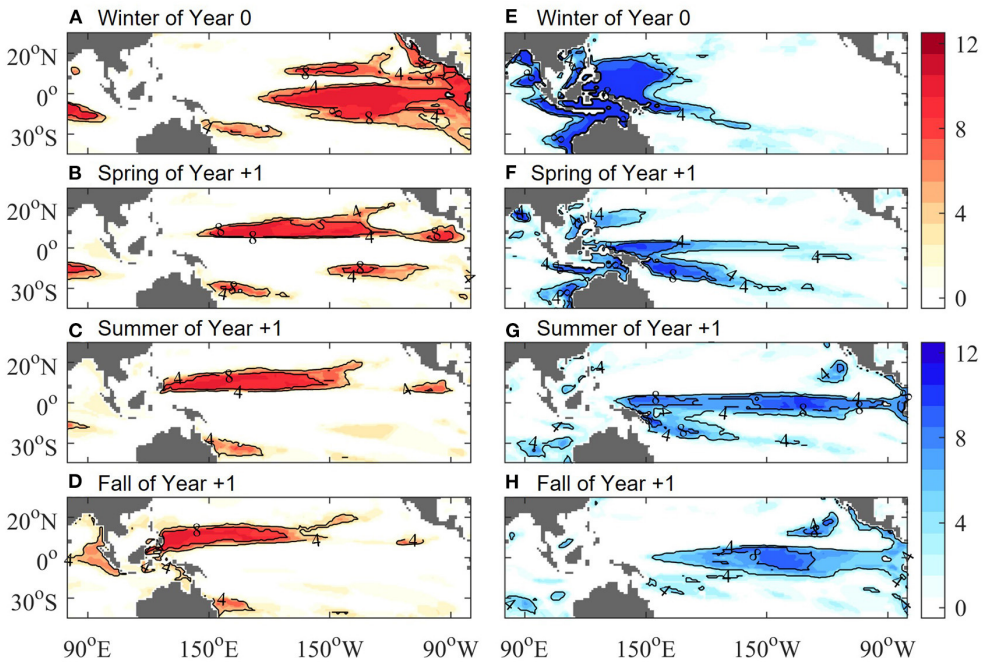

FIGURE 15
Numbers of ensemble members of the CNRM-CM5 model with significant positive correlations between the WEP SZWA in fall and the tropical Indo-Pacific Oceans SSHA in **(A)** winter of Year +0, **(B)** spring of Year +1, **(C)** summer of Year +1, and **(D)** fall of Year +1. **(E–H)** are same as **(A–D)**, but for significant negative correlations.

Data availability statement

Publicly available datasets were analyzed in this study. This data can be found here: The HadISST sea surface temperature data are available at https://www.metoffice.gov.uk/hadobs/hadisst/data/download.html. The AVISO sea surface height data are available at http://www.aviso.altimetry.fr/duacs. The Twentieth Century Reanalysis Project version 3 (20CRv3) dataset is provided by the U.S. Department of Energy, Office of Science Biological and Environmental Research (BER), by the National Oceanic and Atmospheric Administration Climate Program Office, and by the NOAA Physical Sciences Laboratory at https://psl.noaa.gov/data/gridded/data.20thC_ReanV3.html. The EN4 quality controlled ocean data (EN.4.2.1) is provided by the Met Office Hadley Centre at https://www.metoffice.gov.uk/hadobs/en4/download-en4-2-1.html. The CMIP5 output data are available at https://esgf-node.llnl.gov/projects/cmip5/.

Author contributions

TX and DY conceptualized the research. TX executed the research and drafted the manuscript. JW processed the CMIP5 data. All authors contributed to the article and approved the submitted version.

Funding

This study was jointly supported by the National Key Research and Development Program of China (2020YFA0608800), the MNR Program on Global Change and Air-Sea interactions (GASI-04-WLHY-03), and NSFC (Grant Nos. 42076023, 91858204, 41720104008). DY was supported by the Taishan Scholar Program, the National Key Research and Development Program of China (2019YFC1509102), and the Kunpeng Outstanding Scholar Program of the FIO/NMR of China. TX was supported by the Marine S&T Fund of Shandong Province for Pilot National Laboratory for Marine Science and Technology (Qingdao) (2022QNLM010304).

Acknowledgments

We thank the climate modeling groups for producing and making available their model output, the Earth System Grid Federation (ESGF) for archiving the data and providing access, and the multiple funding agencies who support CMIP5 and ESGF.

Conflict of interest

The authors declare that the research was conducted in the absence of any commercial or financial relationships that could be construed as a potential conflict of interest.

Publisher's note

Supplementary material

The Supplementary Material for this article can be found online at: https://www.frontiersin.org/articles/10.3389/fclim.2022.996343/full#supplementary-material

References

Abram, N. J., Gagan, M. K., Cole, J. E., Hantoro, W. S., and Mudelsee, M. (2008). Recent intensification of tropical climate variability in the Indian Ocean. *Nat. Geosci.* 1, 849–853. doi: 10.1038/ngeo357

Alexander, M. A., Bladé, I., Newman, M., Lanzante, J. R., Lau, N. C., and Scott, J. D. (2002). The atmospheric bridge: the influence of ENSO teleconnections on air–sea interaction over the global oceans. *J. Clim.* 15, 2205–2231. doi: 10.1175/1520-0442(2002)015<2205:TABTIO>2.0.CO;2

An, S. I., Hsieh, W. W., and Jin, F. F. (2005). A nonlinear analysis of the ENSO cycle and its interdecadal changes. *J. Clim.* 18, 3229–3239. doi: 10.1175/JCLI3466.1

Annamalai, H., Xie, S. P., McCreary, J. P., and Murtugudde, R. (2005). Impact of Indian Ocean sea surface temperature on developing El Niño. *J. Clim.* 18, 302–319. doi: 10.1175/JCLI-3268.1

Ashok, K., Chan, W. L., Motoi, T., and Yamagata, T. (2004). Decadal variability of the Indian Ocean Dipole. *Geophys. Res. Lett.* 31, L24207. doi: 10.1029/2004GL021345

Behera, S. K., Luo, J. J., Masson, S., Rao, S. A., Sakuma, H., and Yamagata, T. (2006). A CGCM study on the interaction between IOD and ENSO. *J. Clim.* 19, 1688–1705. doi: 10.1175/JCLI3797.1

Bellenger, H., Guiyardi, E., Leloup, J., Lengaigne, M., and Vialard, J. (2014). ENSO representation in climate models: from CMIP3 to CMIP5. *Clim. Dyn.* 42, 1999–2018 doi: 10.1007/s00382-013-1783-z

Bjerknes, J. (1969). Atmospheric teleconnections from the equatorial Pacific. *Monthly Weat. Rev.* 97, 163–172. doi: 10.1175/1520-0493(1969)097<0163:ATFTEP>2.3.CO;2

Cai, W. J., Meyers, G., and Shi, G. (2005). Transmission of ENSO signal to the Indian Ocean. *Geophys. Res. Lett.* 32, L05616. doi: 10.1029/2004GL021736

Castaño-Tierno, A., Mohino, E., Rodríguez-Fonseca, B., and Losada, T. (2018). Revisiting the CMIP5 thermocline in the equatorial Pacific and Atlantic Oceans. *Geophys. Res. Lett.* 12, 963–971. doi: 10.1029/2018GL079847

Chowdary, J. S., and Gnanaseelan, C. (2007). Basin wide warming of the Indian Ocean during El Niño and Indian Ocean dipole years. *Int. J. Climatol.* 27, 1421–1438. doi: 10.1002/joc.1482

Chowdary, J. S., Xie, S. P., Tokinaga, H., Okumura, Y. M., Kubota, H., Johnson, N. C., et al. (2012). Interdecadal variations in ENSO teleconnection to the Indo-western Pacific for 1870-2007. *J. Clim.* 25, 1722–1744. doi: 10.1175/JCLI-D-11-00070.1

Clarke, A. J., and Van Gorder, S. (2003). Improving El Niño prediction using a space-time integration of Indo-Pacific winds and equatorial Pacific upper ocean heat content. *Geophys. Res. Lett.* 30, 1399. doi: 10.1029/2002GL016673

Du, Y., Xie, S. P., Huang, G., and Hu, K. M. (2009). Role of air–sea interaction in the long persistence of El Niño–induced North Indian Ocean warming. *J. Clim.* 22, 2023–2038. doi: 10.1175/2008JCLI2590.1

Du, Y., Xie, S. P., Yang, Y. L., Zheng, X. T., Liu, L., and Huang, G. (2013). Indian Ocean variability in the CMIP5 multimodel ensemble: the Basin Mode. *J. Clim.* 26, 7240–7266. doi: 10.1175/JCLI-D-12-00678.1

Duan, J., Li, Y., Zhang, L., and Wang, F. (2020). Impacts of the Indian Ocean dipole on sea level and gyre circulation of the Western Tropical Pacific Ocean. *J. Clim.* 33, 4207–4228. doi: 10.1175/JCLI-D-19-0782.1

Ducet, N., Le Traon, P. Y., and Reverdin, G. (2000). Global high-resolution mapping of ocean circulation from TOPEX/Poseidon and ERS-1 and−2. *J. Geophys. Res.* 105, 19477–19498. doi: 10.1029/2000JC900063

Gershunov, A., and Barnett, T. (1998). Interdecadal modulation of ENSO teleconnection. *Bull. Am. Meteorol. Soc.* 79, 2715–2725. doi: 10.1175/1520-0477(1998)079<2715:IMOET>2.0.CO;2

Gnanaseelan, C., Deshpande, A., and McPhaden, M. J. (2012). Impact of Indian Ocean Dipole and El Niño/Southern Oscillation wind-forcing on the Wyrtki jets. *J. Geophys. Res.* 117, C08005. doi: 10.1029/2012JC007918

Good, S. A., Martin, M. J., and Rayner, N. A. (2013). EN4: quality controlled ocean temperature and salinity profiles and monthly objective analyses with uncertainty estimates. *J. Geophys. Res. Oceans* 118, 6704–6716. doi: 10.1002/2013JC009067

Ha, K. J., Chu, J. E., Lee, J. Y., and Yun, K. S. (2017). Interbasin coupling between the tropical Indian and Pacific Ocean on interannual timescale: observation and CMIP5 reproduction. *Clim. Dyn.* 48, 459–475. doi: 10.1007/s00382-016-3087-6

Ham, Y. G., and Kug, J. S. (2014). ENSO phase-locking to the boreal winter in CMIP3 and CMIP5 models. *Clim. Dyn.* 43, 305–318. doi: 10.1007/s00382-014-2064-1

Hastenrath, S. (2002). Dipoles, temperature gradients, and ttropical climate anomalies. *Bull. Ame. Meteorol. Soc.* 83, 735–738. doi: 10.1175/1520-0477(2002)083<0735:WLACNM>2.3.CO;2

Huang, G., Hu, K. M., and Xie, S. P. (2010). Strengthening of tropical Indian Ocean teleconnection to the northwest Pacific since the Mid-1970s: an atmospheric GCM study. *J. Clim.* 23, 5294–5304. doi: 10.1175/2010JCLI3577.1

Izumo, T., Legaigne, M., Vialard, J., Luo, J. J., Yamagata, T., and Madec, G. (2014). Influence of the Indian Ocean Dipole and Pacific recharge on following year's El Niño: interdecadal robustness. *Clim. Dyn.* 42, 291–310. doi: 10.1007/s00382-012-1628-1

Izumo, T., Vialard, J., Dayan, H., Lengaigne, M., and Suresh, I. (2016). A simple estimation of equatorial Pacific response from windstress to untangle Indian Ocean Dipole and Basin influences on El Niño. *Clim. Dyn.* 46, 2247–2268. doi: 10.1007/s00382-015-2700-4

Izumo, T., Vialard, J., Lengaigne, M., de Boyer Montegut, C., Behera, S. K., Luo, J. J., et al. (2010). Influence of the Indian Ocean Dipole on following year's El Niño. *Nat. Geosci.* 3, 168–172. doi: 10.1038/ngeo760

Jourdain, N. C., Lengaigne, M., Vialard, J., Izumo, T., and Sen Gupta, A. (2016). Further insights on the influence of the Indian ocean dipole on the following year's ENSO from observations and CMIP5 models. *J. Clim.* 29, 637–658. doi: 10.1175/JCLI-D-15-0481.1

Kajtar, J. B., Santoso, A., England, M. H., and Cai, W. (2015). Indo-Pacific climate interactions in the absence of an Indonesian throughflow. *J. Clim.* 28, 5017–5029. doi: 10.1175/JCLI-D-14-00114.1

Kajtar, J. B., Santoso, A., England, M. H., and Cai, W. (2017). Tropical climate variability: interactions across the Pacific, Indian, and Atlantic Oceans. *Clim. Dyn.* 48, 2173–2190. doi: 10.1007/s00382-016-3199-z

Kug, J. S., and Ham, Y. G. (2012). Indian Ocean feedback to the ENSO transition in a multi-model ensemble. *J. Clim.* 25, 6942–6957. doi: 10.1175/JCLI-D-12-00078.1

Kug, J. S., and Kang, I. S. (2006). Interactive feedback between the Indian Ocean and ENSO. *J. Clim.* 19, 1784–1801. doi: 10.1175/JCLI3660.1

Kug, J. S., Li, T., An, S. I., Kang, I. S., Luo, J. J., Masson, S., et al. (2006). Role of the ENSO–Indian Ocean coupling on ENSO variability in a coupled GCM. *Geophys. Res. Lett.* 33, L09710. doi: 10.1029/2005GL024916

Lau, N. C., and Nath, M. J. (2003). Atmosphere–ocean variations in the Indo-Pacific sector during ENSO episodes. *J. Clim.* 16, 3–20. doi: 10.1175/1520-0442(2003)016<0003:AOVITI>2.0.CO;2

Leloup, J. A., Lachkar, Z., Boulanger, J. P., and Thiria, S. (2007). Detecting decadal changes in ENSO using neural networks. *Clim. Dyn.* 28, 147–162. doi: 10.1007/s00382-006-0173-1

Li, M., Gordon, A. L., Gruenburg, L. K., Wei, J., and Yang, S. (2020). Interannual to decadal response of the Indonesian throughflow vertical profile to Indo-Pacific forcing. *Geophys. Res. Lett.* 47, e2020GL087679. doi: 10.1029/2020GL087679

Li, M., Gordon, A. L., Wei, J., Gruenburg, L. K., and Jiang, G. (2018). Multi-decadal timeseries of the Indonesian throughflow. *Dyn. Atmos. Oceans* 81, 84–95. doi: 10.1016/j.dynatmoce.2018.02.001

Liu, L., Xie, S. P., Zheng, X. T., Li, T., Du, Y., Huang, G., et al. (2014). Indian Ocean variability in the CMIP5 multi-model ensemble: the zonal dipole mode. *Clim. Dyn.* 43, 1715–1730. doi: 10.1007/s00382-013-2000-9

Luo, J. J., Zhang, R. C., Behera, S., Masumoto, Y., Jin, F. F., Lukas, R., et al. (2010). Interaction between El Niño and extreme Indian Ocean dipole. *J. Clim.* 23, 726–742. doi: 10.1175/2009JCLI3104.1

Mukhopadhyay, S., Gnanaseelan, C., Chowdary, J. S., Parekh, A., and Mohapatra, S. (2022). Prolonged La Niña events and the associated heat distribution in the Tropical Indian Ocean. *Clim. Dyn.* 58, 2351–2369. doi: 10.1007/s00382-021-06005-2

Nagura, M., and McPhaden, M. J. (2014). Zonal momentum budget along the equator in the Indian Ocean from a high resolution ocean general circulation model. *J. Geophys. Res. Oceans* 119, 4444–4461 doi: 10.1002/2014JC009895

Ohba, M., Nohara, D., and Ueda, H. (2010). Simulation of asymmetric ENSO transition in WCRP CMIP3 multi-model experiments. *J. Clim.* 23, 6051–6067. doi: 10.1175/2010JCLI3608.1

Philander, S. G. (1990). *El Niño, La Niña, and the Southern Oscillation*. San Diego: Academic Press.

Rayner, N. A., Parker, D. E., Horton, E. B., Folland, C. K., Alexander, L. V., Rowell, D. P., et al. (2003). Global analyses of sea surface temperature, sea ice, and night marine air temperature since the late nineteenth century. *J. Geophys. Res.* 108, 4407. doi: 10.1029/2002JD002670

Saji, N. H., Goswami, B. N., Vinayachandran, P. N., and Yamagata, T. (1999). A dipole mode in the tropical Indian Ocean. *Nature* 401, 360–363. doi: 10.1038/43854

Sang, Y. F., Singh, V. P., and Xu, K. (2019). Evolution of IOD-ENSO relationship at multiple time scales. *Theoret. Appl. Climatol.* 136, 1303–1309. doi: 10.1007/s00704-018-2557-7

Santoso, A., England, M. H., and Cai, W. (2012). Impact of Indo-Pacific feedback interactions on ENSO dynamics diagnosed using ensemble climate simulations. *J. Clim.* 25, 7743–7763. doi: 10.1175/JCLI-D-11-00287.1

Slivinski, L. C., Compo, G. P., Whitaker, J. S., Sardeshmukh, P. D., Giese, B. S., McColl, C., et al. (2019). Towards a more reliable historical reanalysis: Improvements for version 3 of the Twentieth Century Reanalysis system. *Q. J. R. Meteorol. Soc.* 145, 2876–2908. doi: 10.1002/qj.3598

Song, Q., Vecchi, G. A., and Rosati, A. (2008). Predictability of the Indian Ocean sea surface temperature anomalies in the GFDL coupled model. *Geophys. Res. Lett.* 35, L02701. doi: 10.1029/2007GL031966

Stuecker, M. F., Timmermann, A., Jin, F.F., Chikamoto, Y., Zhang, W., Wittenberg, A. T., Widiasih, E., and Zhao, S. (2017). Revisiting ENSO/Indian Ocean Dipole phase relationships. *Geophys. Res. Lett.* 44, 2481–2492. doi: 10.1002/2016GL072308

Tao, W. C., Huang, G., Hu, K. M., Qu, X., Wen, G. H., and Gong, H. N. (2015). Interdecadal modulation of ENSO teleconnections to the Indian Ocean Basin Mode and their relationship under global warming in CMIP5 models. *Int. J. Climatol.* 35, 391–407. doi: 10.1002/joc.3987

Taylor, K. E., Stouffer, R. J., and Meehl, G. A. (2012). An overview of CMIP5 and the experiment design. *Bull. Am. Meteorol. Soc.* 93, 485–498. doi: 10.1175/BAMS-D-11-00094.1

Tillinger, D., and Gordon, A. L. (2010). Fifty years of the Indonesian throughflow. *J. Clim.* 22, 6342–6355. doi: 10.1175/2009JCLI2981.1

Trenberth, K. E., and Zhang, Y. X. (2019). Observed interhemispheric meridional heat transports and the role of the Indonesian Throughflow in the Pacific Ocean. *J. Clim.* 32, 8523–8536. doi: 10.1175/JCLI-D-19-0465.1

Ummenhofer, C. C., Sen Gupta, A., Li, Y., Taschetto, A. S., and England, M. H. (2011). Multi-decadal modulation of the El Niño-Indian monsoon

relationship by Indian Ocean variability. *Environ. Res. Lett.* 6, 034006. doi: 10.1088/1748-9326/6/3/034006

Wang, C. (2019). Three-ocean interactions and climate variability: a review and perspective. *Clim. Dyn.* 53, 5119–5136. doi: 10.1007/s00382-019-04930-x

Wang, C., and Picaut, J. (2004). "Understanding ENSO physics-a review," in *Earth's Climate: The Oceanatmosphere Interaction. AGU Geophysical Monograph Series*, eds C. Wang, S. P. Xie, and J. A. Carton (Washington D.C.: American Geophysical Union), 21–48.

Wang, J., Yuan, D., and Zhao, X. (2021). Comparison of the positive and negative Indian Ocean Dipole forcing on the Pacific interannual variability through the oceanic channel. *J. Oceanogr.* 77, 819–826. doi: 10.1007/s10872-021-00611-8

Webster, P. J., Moore, A. M., Loschnigg, J. P., and Leben, R. R. (1999). Coupled ocean–atmosphere dynamics in the Indian Ocean during 1997-1998. *Nature* 401, 356–360. doi: 10.1038/43848

Wu, R., and Kirtman, B. P. (2004). Understanding the impacts of the Indian Ocean on ENSO variability in a coupled GCM. *J. Clim.* 17, 4019–4031. doi: 10.1175/1520-0442(2004)017<4019:UTIOTI>2.0.CO;2

Xie, S. P., Du, Y., Huang, G., Zheng, X. T., Tokinaga, H., Hu, K. M., et al. (2010). Decadal shift in El Niño influences on Indo-Western Pacific and East Asian Climate in the 1970s. *J. Clim.* 23, 3352–3368. doi: 10.1175/2010JCLI3429.1

Xie, S. P., Hu, K., Hafner, J., Tokinaga, H., Du, Y., Huang, G., et al. (2009). Indian Ocean capacitor effect on Indo-western Pacific climate during the summer following El Niño. *J. Clim.* 22, 730–747. doi: 10.1175/2008JCLI2544.1

Xu, T. F., and Yuan, D. L. (2014). Why does the IOD-ENSO teleconnection disappears in some decades? *Chin. J. Oceanol. Limnol.* 33, 534–544. doi: 10.1007/s00343-015-4044-7

Xu, T. F., Yuan, D. L., Yu, Y. Q., and Zhao, X. (2013). An assessment of the Indo-Pacific oceanic channel dynamics in the FGOALS-g2 coupled climate system model. *Adv. Atmosp. Sci.* 30, 997–1016. doi: 10.1007/s00376-013-2131-2

Yamagata, T., Behera, S. K., Rao, S. A., Guan, Z., Ashok, K., and Saji, H. N. (2003). Comments on "Dipoles, temperature gradients, and tropical climate anomalies". *Bull. Am. Meteorol. Soc.* 84, 1418–1422. doi: 10.1175/BAMS-84-10-1418

Yang, Y., Xie, S. P., Wu, L. X., Kosaka, Y., Lau, N. C., and Vecchi, G. A. (2015). Seasonality and predictability of the Indian Ocean dipole mode: ENSO forcing and internal variability. *J. Clim.* 28, 8021–8036. doi: 10.1175/JCLI-D-15-0078.1

Yuan, D., Hu, X., Xu, P., Zhao, X., Masumoto, Y., and Han, W. (2018). The IOD-ENSO precursory teleconnection over the tropical Indo-Pacific Ocean: dynamics and long-term trends under global warming. *J. Oceanol. Limnol.* 36, 4–19. doi: 10.1007/s00343-018-6252-4

Yuan, D. L., Wang, J., Xu, T. F., Xu, P., Zhou, H., Zhao, X., et al. (2011). Forcing of the Indian Ocean dipole on the interannual variations of the Tropical Pacific ocean: roles of the Indonesian throughflow. *J. Clim.* 15, 3597–3608. doi: 10.1175/2011JCLI3649.1

Yuan, D. L., Zhou, H., and Zhao, X. (2013). Interannual climate variability over the tropical Pacific Ocean induced by the Indian Ocean dipole through the Indonesian throughflow. *J. Clim.* 26, 2845–2861. doi: 10.1175/JCLI-D-12-00117.1

Yuan, Y., and Li, C. Y. (2008). Decadal variability of the IOD-ENSO relationship. *Chin. Sci. Bull.* 53, 1746–1752. doi: 10.1007/s11434-008-0196-6

Zhang, L. Y., Du, Y., Tozukam, T., and Kido, S. (2021). Revisiting ENSO impacts on the Indian Ocean SST based on a combined linear regression method. *Acta Oceanol. Sin.* 40, 47–57. doi: 10.1007/s13131-021-1733-2

Zhao, X., Yuan, D., Yang, G., Zhou, H., and Wang, J. (2016). Role of the oceanic channel in the relationships between the basin/dipole mode of SST anomalies in the tropical Indian Ocean and ENSO transition. *Adv. Atmosp. Sci.* 33, 1386–1400. doi: 10.1007/s00376-016-6048-4

Zheng, X. T., Xie, S. P., Du, Y., Liu, L., Huang, G., and Liu, Q. Y. (2013). Indian Ocean Dipole response to global warming in the CMIP5 multimodel ensemble. *J. Clim.* 26, 6067–6080. doi: 10.1175/JCLI-D-12-00638.1

Zhou, Q., Duan, W., and Hu, J. (2020). Exploring sensitive area in the tropical Indian Ocean for El Niño prediction: implication for targeted observation. *J. Oceanol. Limnol.* 1602–1615. doi: 10.1007/s00343-019-9062-4

Zhou, Q., Duan, W. S., Mu, M., and Feng, R. (2015). Influence of positive and negative Indian Ocean Dipoles on ENSO via the Indonesian throughflow: results from sensitivity experiments. *Adv. Atmosp. Sci.* 32, 783–793. doi: 10.1007/s00376-014-4141-0

Zhou, Q., Duan, W. S., Wang, X., Li, X., and Zu, Z. Q. (2021). The initial errors in the tropical Indian Ocean that can induce a significant "Spring Predictability Barrier" for La Niña events and their implication for targeted observations. *Adv. Atmosp. Sci.* 38, 1566–1579. doi: 10.1007/s00376-021-0427-1

Zhou, Q., Mu, M., and Duan, W. (2019). The initial condition errors occurring in the Indian Ocean temperature that cause "spring predictability barrier" for El Niño in the Pacific Ocean. *J. Geophys. Res. Oceans* 124, 1244–1261. doi: 10.1029/2018JC014403